

Article

Structural and Dynamic Characterization of Li-Ionic Liquid Electrolyte Solutions for Application in Li-Ion Batteries: A Molecular Dynamics Approach

Michele A. Salvador ^{1,*}, Rita Maji ², Francesco Rossella ^{1,3}, Elena Degoli ^{3,4,5}, Alice Ruini ^{1,3,5} and Rita Magri ^{1,3,5,*}

- ¹ Dipartimento di Scienze Fisiche, Informatiche e Matematiche, Università di Modena e Reggio Emilia, Via Campi 213/A, 41125 Modena, Italy
 - ² Dipartimento di Scienze e Metodi dell'Ingegneria, Università di Modena e Reggio Emilia, Via Amendola 2 Padiglione Tamburini, 42122 Reggio Emilia, Italy
 - ³ Centro S3, Istituto Nanoscienze-Consiglio Nazionale delle Ricerche (CNR-NANO), Via Campi 213/A, 41125 Modena, Italy
 - ⁴ Dipartimento di Scienze e Metodi dell'Ingegneria, Università di Modena e Reggio Emilia and Centro Interdipartimentale En&Tech, Via Amendola 2 Padiglione Morselli, 42122 Reggio Emilia, Italy
 - ⁵ Centro Interdipartimentale di Ricerca e per i Servizi nel Settore Della Produzione, Stoccaggio ed Utilizzo dell'Idrogeno H2-MO.RE., Via Università 4, 41121 Modena, Italy
- * Correspondence: michelesalvador@gmail.com (M.A.S.); rita.magri@unimore.it (R.M.)

Abstract: Pyrrolidinium-based (Pyr) ionic liquids (ILs) have been proposed as electrolyte components in lithium-ion batteries (LiBs), mainly due to their higher electrochemical stability and wider electrochemical window. Since they are not naturally electroactive, in order to allow their use in LiBs, it is necessary to mix the ionic liquids with lithium salts (Li). Li-PF₆, Li-BF₄, and Li-TFSI are among the lithium salts more frequently used in LiBs, and each anion, namely PF₆ (hexafluorophosphate), BF₄ (tetrafluoroborate), and TFSI (bis(trifluoromethanesulfonyl)azanide), has its own solvation characteristics and interaction profile with the pyrrolidinium ions. The size of Pyr cations, the anion size and symmetry, and cation–anion combinations influence the Li-ion solvation properties. In this work, we used molecular dynamics calculations to achieve a comprehensive view of the role of each cation–anion combination and of different fractions of lithium in the solutions to assess their relative advantage for Li-ion battery applications, by comparing the solvation and structural properties of the systems. This is the most-comprehensive work so far to consider pyrrolidinium-based ILs with different anions and different amounts of Li: from it, we can systematically determine the role of each constituent and its concentration on the structural and dynamic properties of the electrolyte solutions.

Keywords: electrolyte solutions; transference number; structural properties



check for updates

Citation: Salvador, M.A.; Maji, R.; Rossella, F.; Degoli, E.; Ruini, A.; Magri, R. Structural and Dynamic Characterization of Li-Ionic Liquid Electrolyte Solutions for Application in Li-Ion Batteries: A Molecular Dynamics Approach. *Batteries* **2023**, *9*, 234. <https://doi.org/10.3390/batteries9040234>

Academic Editor: Junnan Hao

Received: 27 February 2023

Revised: 29 March 2023

Accepted: 10 April 2023

Published: 19 April 2023



Copyright: © 2023 by the authors. Licensee MDPI, Basel, Switzerland. This article is an open access article distributed under the terms and conditions of the Creative Commons Attribution (CC BY) license (<https://creativecommons.org/licenses/by/4.0/>).

1. Introduction

Ionic liquids (ILs) are a set of ionic compounds that remain liquid at room temperature or close to it, with melting temperatures normally in the range 25–100 °C [1]. They are usually formed by an organic, bulky, and asymmetric cation and an inorganic or organic and symmetric anion. Initially used as solvents, ionic liquids can now be employed in a large variety of applications, such as gas storage, lubricants, sensors, reaction media, and lithium batteries, among others [2–7]. The molecular structure of the cations, composed by a delocalized charge moiety such as imidazolium, pyridinium, pyrrolidinium, or ammonium, among others, bonded to a flexible organic chain with different lengths can be combined with anions of different sizes, shapes, orientations, and complexities. The combination induces a self-organization and determines the physical and transport properties of the species in the ionic liquid [8–13]. A lower volatility and flammability and a good chemical

and thermal stability compared to traditional solvents make ionic liquids interesting for application in batteries, often in conjunction with polymeric chains [14–17].

Pyrrolidinium-based ionic liquids (Pyr1X-anion) have been proposed as electrolyte components in lithium-ion batteries (LiBs), mainly due to their higher electrochemical stability and wider electrochemical window [18–21]. Besides, pyrrolidinium cations have been extensively pointed out as appropriate for use in LiBs due to their versatility, allowing combinations with different anions [20,22]. Their action has been reported to be very sensitive to changes in their lateral chains [3,23–25]. However, they are not naturally electroactive, and in order to allow their use in LiBs, it is necessary to mix the ionic liquids with lithium salts [26,27].

The performance of the ionic liquid–Li-ion electrolyte solutions is related to the mobility of the Li-ions and is thus closely affected by the Li-ion local environment, i.e., its solubility and solvation properties. Moreover, it is important to understand how the lithium salts affect the electrode–IL interface [28,29]. According to the literature [26], lithium mobility in the ionic liquid is mainly ruled by two mechanisms: (i) the vehicular mechanism, where Li^+ moves together with its anionic solvation shell, and (ii) the exchange mechanism, where Li^+ moves by jumping from one solvation shell to another [26,30]. The predominance of one mechanism above the other is reported as being dependent on the interactions among the three species (anion, cation, Li), with the vehicular one seeming to be the most-significant. Along with an improvement of the Li-ion mobility with the increment of the lithium content, an increase in the viscosity and density of the electrolyte solution has also been reported [27,29,31–33]. These variations are also related to the temperature, and they have different trends for different cation–anion combinations.

Li–PF₆, Li–BF₄, and Li–TFSI are among the lithium salts more frequently used in Li-ion batteries, and each anion, namely PF₆ (hexafluorophosphate), BF₄ (tetrafluoroborate) and TFSI (bis(trifluoromethanesulfonyl)azanide or bis(trifluoromethane)sulfonimide, also referred to as NTf_2) has its own solvation characteristics and interaction profile with the pyrrolidinium ions. PF₆ is reported as having a small temperature range for applications, since it is subject to degradation at temperatures larger than 60 °C, while it crystallizes at lower temperatures (–20 °C) [20]. BF₄ does not present such temperature limitations, tends to improve the transport properties, and has been used for probing electrolyte interactions since it tends to form bonds with the Li-ions of an intermediate strength relative to the Li–PF₆ and Li–TFSI bonds [34]. Li–TFSI is the most-used lithium salt because the negative charges are more dispersed throughout the anion sulfonyl groups, and the interactions with the lithium ions are weaker, allowing for an improved diffusivity [20,33].

Canongia López and coworkers reported in 2004 [35] a systematic study using interaction parameters based on the OPLS-AA [36] and Amber [37] force fields to model ionic liquids formed by the 1-alkyl-3-methylimidazolium cation and the most-common anions (i.e., BF₄, PF₆, Cl, etc.). These results were validated by comparing the resulting density with the experimental results, showing good agreement. The group extended their studies to include pyridinium, phosphonium [38], and pyrrolidinium [39] cations, and all these results were compiled in a model called the CL&P force field [40]. Although extensively used and considered successful to obtain structural properties, this force field and similar ones fail in explaining dynamic properties such as self-diffusion, viscosity, and conductivity. This is probably related to the overestimation of the electrostatic interactions, which cause a considerable charge ordering, due to the fact that these classical force fields do not take into account charge transfers and polarization effects [41].

Borodin and coworkers [2] developed a polarizable force field used to obtain both the structural and dynamic properties of a wide variety of ionic liquids. The essential difference with the the Canongia Lopes model is that, besides the intramolecular (bonds, angles, and dihedrals) and intermolecular (van der Waals and electrostatic) energy terms, it includes a polarization energy term, which comes from the interaction between induced dipoles. In a similar approach, i.e., taking into account a polarization term, McDaniel and coworkers [42] proposed an ab-initio-derived forcefield to study imidazolium-based ionic liquids. In both

studies, this methodology showed results in good agreement with the experimental ones, especially for the dynamic properties. However, it increased significantly the computational cost of the simulations.

Alternatives have been proposed to reproduce the dynamic properties. Among them, we mention the optimization of the van der Waals parameters [43], the use of scaled charge models [44,45], or performing the calculations at high temperatures [8]. In particular, the scaled charge models, which consist of using a fraction of the atomic partial charges instead of the full ones for each ion (i.e., 0.5–0.9 |e|), showed good agreement with the experimental results. Their results compared also favorably in comparison with the polarizable force field models, especially for the structural properties. The theoretical justification for using the partial charge method is that it mimics the charge transfer between the ions, and albeit that it is capable of accurately reproducing the properties of neat ionic liquids, it becomes problematic when one has to consider other solute elements in the simulation, such as monoatomic ions and organic molecules. This is due to the fact that the choice of applying or not the charge scaling to the solute entities is not trivial [41].

Considering the different models described and the nature of our systems, we chose to use the Canongia Lopes intramolecular and intermolecular parameters for cations and anions, recalculating the partial charges after proper minimization and vibrational frequency calculations. We used a full-charge model ($q = +1.0$ for the pyrrolidinium cations and Li, $q = -1.0$ for the anions), since among the species considered, we have Cl and Li, both monoatomic. This choice was made because of the amount of species we considered, neat and with different fractions of Li, which resulted in a large number of calculations. Therefore, the classical force field with a full-charge model provided us with the appropriate tool for building a broad picture by isolating the effects of each variable, while keeping, at the same time, the computational cost within reasonable bounds.

In order to achieve an understanding of the role of each variable that determines the interaction profile of the species in the electrolyte solution, we considered ionic liquids (ILs) obtained by combining the pyrrolidinium cations (1,*n*-alkyl-pyrrolidinium) with different alkyl chains (*Pyrr1X* : $X = 2, \dots, 6$) and anions with different sizes and symmetries: the monoatomic chloride (Cl), the quasi-spherical tetrafluoroborate (BF₄) and hexafluorophosphate (PF₆), and the symmetric, but linear-shaped bis(trifluoro-methane) sulfonimide (TFSI). The codes, names, structural formulas, and 3D representations of all species considered in this work are listed in the Supplementary Material: Table S1. We aimed to understand how the structural and dynamic properties vary with the cation–anion combinations. We also analyzed the variations of these properties with the addition of different fractions of lithium and investigated the properties related to the Li conductivity in the ionic liquid–Li electrolyte solutions that would allow them to be applied in Li-ion batteries. In Section 2, we describe the methodology used throughout this paper, the computational details, and the constituents of our systems. In Section 3, we present first the results and discussions for the neat ionic liquids (Section 3.1) and then those relative to the electrolyte solutions, formed by the ionic liquids with different fractions of Li-ions (Section 3.2).

2. Methods and IL Systems

Classical molecular dynamics simulations with an all-atom approach and using periodic boundary conditions in all directions, as implemented in the Gromacs 2020 software [46,47], were used to study the structural and dynamic properties of electrolyte solutions, based on ionic liquids and different amounts of lithium. OPLS-based force field parameters [36] improved by Canongia Lopes [38] were used to model the intramolecular and intermolecular interactions, and Lorentz–Berthelot mixing rules [48] were used to obtain the crossed terms for the non-bonded atoms. In order to treat the long-range electrostatic interactions, the Ewald summation technique [49] was used, with a grid spacing of 12 nm and a cut-off distance 1.6 nm for all systems, and hydrogen bond lengths were constrained using the LINCS algorithm [50]. Self-diffusion of the ionic species was

obtained from the mean-squared displacement (*MSD*) along a time interval *t*, with the Einstein correlation (Equation (1)), where *r*(*t*) are the positions at each time *t*:

$$D = \lim_{t \rightarrow \infty} \langle MSD \rangle = \frac{1}{6t} \lim_{t \rightarrow \infty} \langle |r(t) - r(0)|^2 \rangle \quad (1)$$

The self-diffusion (*D*) allowed us to obtain the transference number, defined as the weighted average of the diffusion of each species that form the system. Therefore, the Li transference number (*t_{Li}*) can be calculated from Equation (2):

$$t_{Li} = \frac{f_{Li} * D_{Li}}{f_{Li} * D_{Li} + f_{cat} * D_{cat} + f_{an} * D_{an}}, \quad (2)$$

where *f_{Li}*, *f_{cat}*, and *f_{an}* are the fractions of the Li, cation, and anion, respectively, and *D_{Li}*, *D_{cat}*, and *D_{an}* are the self-diffusion values of the Li, cation, and anion, respectively.

The individual molecules were built using the Avogadro software [51,52], and the structures were optimized using density functional theory (DFT) calculations, as implemented in the Orca software [53]. Vibrational frequency calculations were performed to verify if the configurations obtained corresponded to the minima in the potential energy surface. Both the optimization and frequency calculations were performed using the B3LYP/G functional [54] and a 6–31g(d) basis set [55]. Partial charges were obtained from an electrostatic surface potential methodology (CHelpG) [56], at the B3LYP//6–31g level of theory. Indeed, for the calculations considering only the ionic liquids, some works in the literature [40,44] mention that a higher level of theory would be more appropriate to account for the cation–anion interactions. However, some works, including recent ones [13,45], have pointed out that B3LYP//6–31g can be considered an appropriate choice, providing enough accuracy on energetics at a lower computational cost [13,39,45], and to date, we have not found any work that extends this benchmark study for ternary electrolyte solutions as those considered in our work.

Pyrrrolidinium-based cations (1-*n*-alkyl-1-methyl-pyrrolidinium) were combined with chloride (Cl), tetrafluoroborate (BF₄), hexafluorophosphate (PF₆), and bis(trifluoromethane) sulfonimide (TFSI) anions to form the so-called neat ionic liquids, while a fraction of the cations were replaced (1:1 proportion) by lithium cations (Li) to form the electrolyte solutions. In this study, we chose to keep the number of ion pairs fixed, 400 ion pairs, and to collect the properties at the same temperature, 400 K. We chose to perform all calculations at a temperature higher than room temperature, in order to obtain reasonable results with shorter trajectories and computational time [8].

The Gromacs pre-processing tools [47] were used to build the simulation boxes, which were obtained by placing randomly the 400 ion pairs in a cubic box. For the minimization phase, we used the steepest-descent [46] algorithm for the first run, followed by an l-bfgs [46] algorithm for the second run. The first equilibration cycle was performed using the leap-frog integrator, with a 1.0 fs time step, using a velocity-rescale thermostat [57] and the Berendsen barostat [46,58] in an isothermal–isobaric (NPT) simulation, followed by an isothermal–isovolumetric (NVT) simulation with the same thermostat. This cycle was performed using 1 bar of pressure and 400 K temperature for all systems. After this phase, an annealing protocol was used, by increasing the temperature up to 700 K and decreasing it to 400 K. A second equilibration cycle was performed after the annealing phase, with (i) an NPT ensemble using the Berendsen barostat [46,58] and a velocity-rescale thermostat [57] (10 ns), (ii) an NPT ensemble with the Parrinello–Rahman barostat [59] and the same thermostat (10 ns), and finally, (iii) an NVT run with the same thermostat, also for 10 ns. For some systems, this protocol was performed one more time in order to achieve an equilibrated configuration. Finally, a 20 ns production phase, also at a 400 K temperature and 1 bar of pressure using the same thermostat and the Parrinello–Rahman barostat, was performed in order to extract the properties of interest. Both the second equilibration cycle and the production run were performed with a 0.5 fs time step.

In this study, we considered ionic liquids (ILs) obtained by combining the following cations: 1-methyl-1-ethyl pyrrolidinium (Pyr12), 1-methyl-1-propyl pyrrolidinium (Pyr13), 1-methyl-1-butyl pyrrolidinium (Pyr14), 1-methyl-1-pentyl pyrrolidinium (Pyr15), and 1-methyl-1-hexyl pyrrolidinium (Pyr16) with the anions: chloride (Cl), tetrafluoroborate (BF₄), hexafluorophosphate (PF₆), and bis(trifluoro- methane)sulfonimide (TFSI), to understand how the structural and dynamic properties vary with the cation–anion combinations. We also analyzed the variations of these properties with the addition of different fractions of lithium and investigated the properties related to the Li conductivity in these ionic liquid–Li electrolyte solutions that would allow them to be applied in Li-ion batteries. Although some of the cation–anion combinations, for example Pyr13–PF₆ and Pyr12–BF₄ [33], present a solid-state phase at lower temperatures (melting points at 200 °C [60] and 280 °C [61], respectively), we nevertheless considered also their combinations in order to have a broad view of the trends of the systems with and without lithium with the anion dimension. Figure 1 shows on the top row three of the pyrrolidinium cations (Pyr12, Pyr14, and Pyr16) and the Li-ion and on the bottom row all the anions we considered in our simulations.

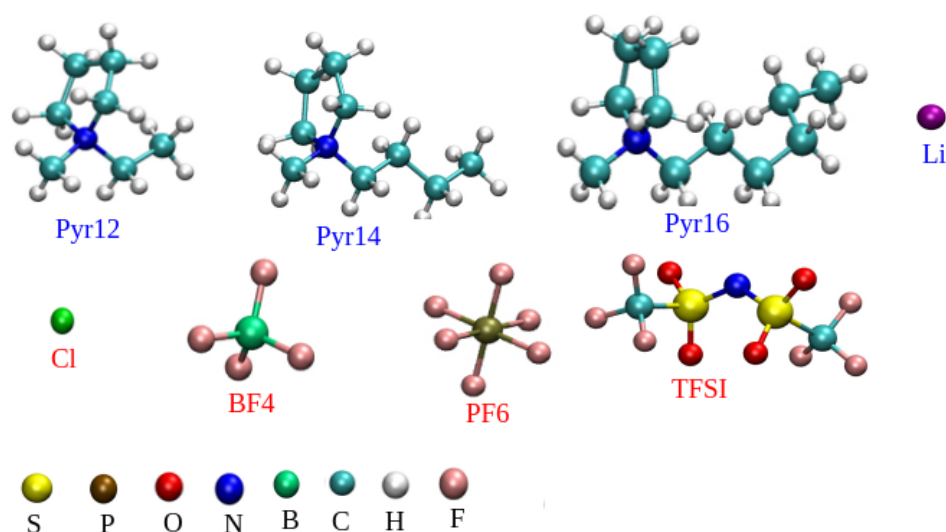


Figure 1. Top row: three of the pyrrolidinium cations (Pyr12, Pyr14, and Pyr16) and the Li-ion; bottom row: anions Cl, BF₄, PF₆, and TFSI.

3. Results and Discussions

3.1. Neat Pyrrolidinium-Anion Ionic Liquids

In this subsection, we present the results of the density, pair correlation function ($g(r)$), and coordination of the neat ionic liquids, considering the pyrrolidinium cations (Pyr1, $X : X = 2, \dots, 6$) in combination with Cl, BF₄, PF₆, and TFSI. Figure 2 shows the IL density as a function of the size of the aliphatic chain of the pyrrolidinium cations, for each anion considered. We can see that the density increased as the size of the anion increased, and it slightly decreased linearly as we increased the cations' carbon chain. Furthermore, the larger the anion, the more significantly the density varied with the size of the cation. We also analyzed the molar mass of each ion, and we observed that the molar mass of the anions changed with the kind of anion more significantly, while for the cations, it varied linearly with the increase of the carbon chain. The molar masses of all species are listed in Table 1 and a graphic representation can be found in the Supplementary Material: Figure S1.

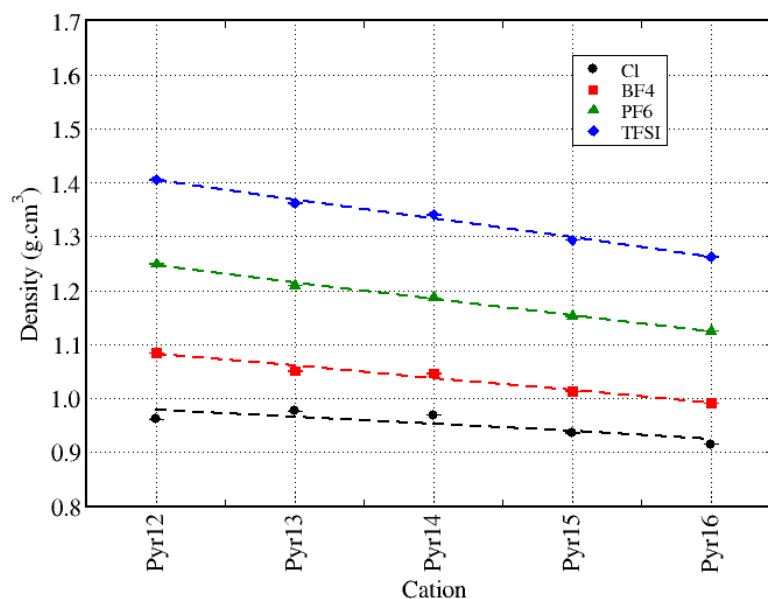


Figure 2. Density of the neat ionic liquids as a function of the size of the pyrrolidinium aliphatic chain, for all anions.

The decrease in density due to the increase of the cation lateral chain has been reported in the literature by many authors [9,33,62–66], for different ionic liquid systems and different cations. R  ther and co-workers [33] discussed in their review on ionic-liquid-based batteries that the properties such as the geometry, charge density, and distribution of the anions will determine the structure of the solvation shell and will influence the density and diffusion of the ions, while the cations will induce a much smaller influence. M  ndez-Morales and coworkers [9] investigated systems with BF₄⁻, PF₆⁻, and TFSI⁻ as the anions, but with only one cation: 1-butyl-3-methylimidazolium (BMIM). They found a trend very similar to ours, with the densities varying in the sequence BF₄⁻ < PF₆⁻ < TFSI⁻, and there was no discussion about the reason for this trend. A similar trend was also reported by Haskings and co-workers [32], which compared the properties of Pyr14–TFSI, Pyr13–FSI (N-methyl-N-propylpyrrolidinium bis(fluorosulfonyl)imide), and EMIM–BF₄ (1-ethyl-3-methylimidazolium boron tetrafluoride). They did not consider all possible cation–anion combinations and did not isolate the effect induced by varying the cation size (Pyr14 > EMIM > Pyr13) or the anion size (TFSI > FSI > BF₄⁻) separately. However, they observed that the density decreased noticeably as the anion size decreased, with Pyr14–TFSI having a larger density than Pyr13–FSI and EMIM–BF₄.

Tong and coworkers [65,67] suggested that the density increases with the number of atoms with larger electronic densities (such as oxygen and fluorine) present in the anions, and it decreases as the length of the cation aliphatic side chain increases. Yamaguchi and coworkers [66] used the parameters ϕ ($\phi = r_{\text{smaller ion}}/r_{\text{larger ion}}$) and shape of the ions to analyze their correlation with the ionic conductivity in plastic ionic liquids, mentioning specifically that this ϕ –conductivity correlation was not necessarily related to the shape (spherical or not) of the ions.

Table 2 presents a comparison between the results obtained in this work and the simulations and/or experimental results found in the literature. It is important to mention that the simulations were performed at different temperatures, and also, the methodologies applied are different. Chaban and co-workers’ results [44] were obtained with the same force field parameters we used, but they used a scaled model for the charges, while we used the full-charge model. Nevertheless, our calculated density for Pyr13–TFSI is in concordance with [44] with a deviation of 2% and with their simulation results for the Pyr14–Cl with a deviation of 6%. Kashyap and co-workers [68] also used the same force field parameters and a scaled charge model for their calculations, and although they used

a lower temperature, we can see that the trend was the same as ours, with the densities decreasing as we increased the size of the carbon lateral chain of Pyr1X.

Table 1. Molar mass of cations and anions.

| Cations | Molar Mass (g/mol) | Anion | Molar Mass (g/mol) |
|---------|--------------------|-----------------|--------------------|
| Pyr12 | 114.2 | Cl | 35.4 |
| Pyr13 | 128.2 | BF ₄ | 86.8 |
| Pyr14 | 142.3 | PF ₆ | 144.9 |
| Pyr15 | 156.3 | TFSI | 280.1 |
| Pyr16 | 170.3 | - | - |

Table 2. Comparison between the density results obtained in this work and the simulation/experimental results found in the literature (density in g·cm⁻³).

| | (400 K) This Work | Haskings [32] (390 K) sim/exp | Chaban [44] (355 K) sim/exp | Kashyap [68] (295 K) sim/exp |
|-----------------------|----------------------|----------------------------------|--------------------------------|---------------------------------|
| Pyr13-TFSI | 1.362 | 1.264/- | -/1.378 | - |
| Pyr14-Cl | 0.969 | -/1.049 | 0.910/- | - |
| Pyr14-BF ₄ | 1.047 | 1.315/1.313 | 1.004/- | - |
| Pyr14-TFSI | 1.341 | - | 1.346/1.398 | 1.453/1.390 |
| Pyr15-TFSI | 1.294 | - | - | 1.418/1.360 |
| Pyr16-TFSI | 1.263 | - | - | 1.387/1.320 |

Figure 3 presents the center-of-mass cation–cation, cation–anion, and anion–anion pair correlation functions ($g(r)$) for the Pyr12–anion and Pyr16–anion. The results for the other pyrrolidinium cations and all the cation–anion combinations can be found in the Supplementary Material: Figures S2 and S3. We observed that the intensity of the first peak of the cation–cation $g(r)$ decreased with the increase of the cation aliphatic chain, and the position and form of the first peak were similar for BF₄ and PF₆ in all cases, except for Pyr12. Indeed, the first peak was always the one related to Pyr1X–Cl, the smaller anion. Furthermore, we can observe that the cation–cation $g(r)$ curves for TFSI are similar, except for Pyr16. When we compared the cation–anion $g(r)$, for Cl and BF₄, the smaller the anion, the closer it was to the cation, for all cations. Furthermore, the intensity of the first peak decreased as well, although to a lesser extent than for the cation–cation $g(r)$. For PF₆ and TFSI, the peaks were closer to each other in the systems with Pyr12 and Pyr13 as cations, while the cation–anion distances increased with the size of the anion, for Pyr14, Pyr15, and Pyr16. We can also see the formation of a second peak close to the first one, for Pyr15 and Pyr16 for all anions, except TFSI, which indicates two preferred near neighbor positions of the cations with respect to the anions. As the cation aliphatic chain increased, the position of this second peak shifted to larger values of r .

Table 3 shows the position of the first peak in the cation–anion $g(r)$ curves, for all the systems considered. We can observe that, for a given anion, the peak position changed at most 0.3 Å as we varied the cation. If we fixed the cation, however, the position of the anion varied in the range of 0.4–1.3 Å. We can summarize our results in this way: (i) the larger the anion, the larger is the cation–anion distance, while (ii) the larger the cation, smaller is the cation–anion distance.

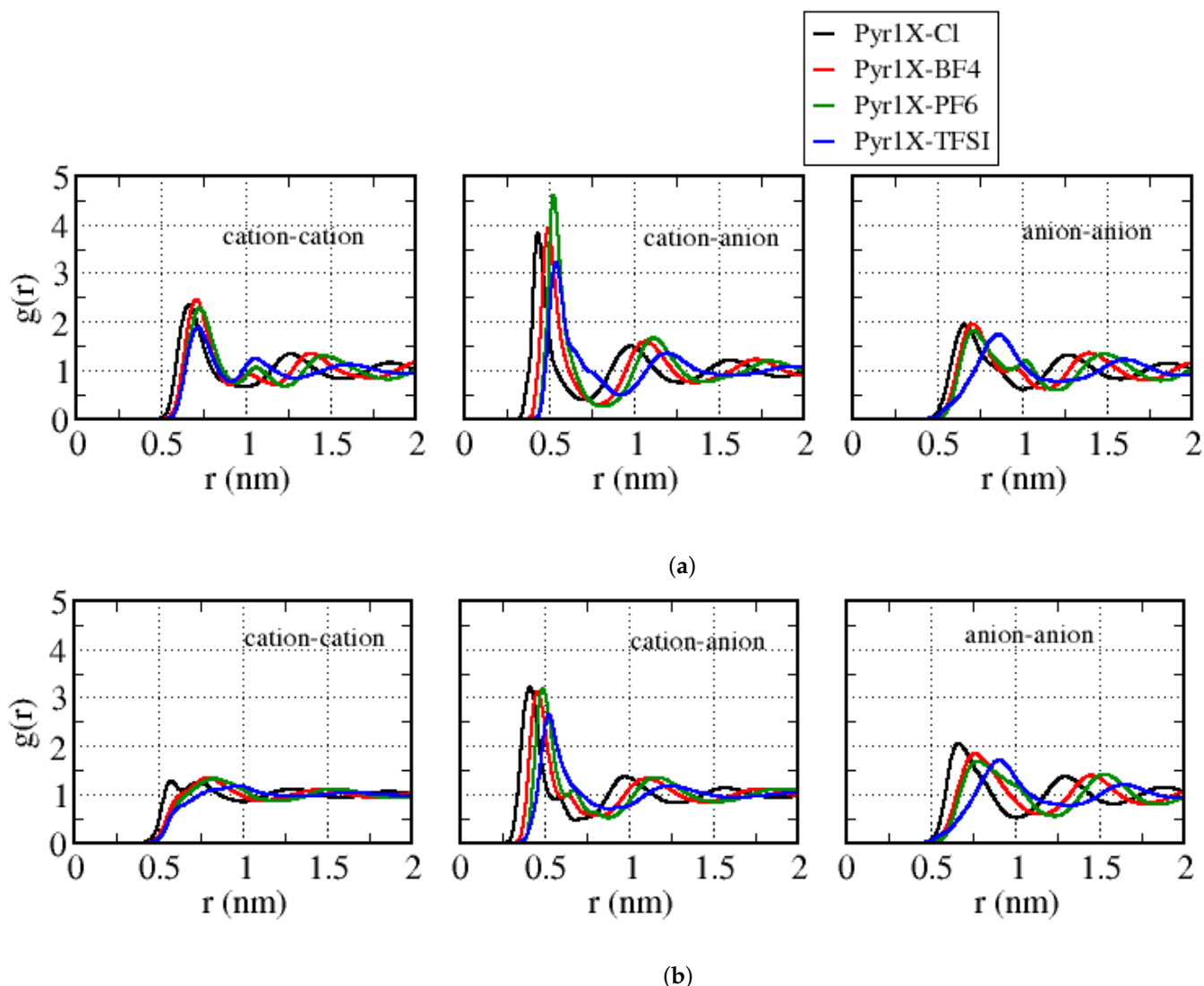


Figure 3. Center-of-mass cation–cation, cation–anion, and anion–anion pair correlation functions ($g(r)$) for all the cation–anion combinations with: (a) Pyr12 as the cation; (b) Pyr16 as the cation.

Table 3. Position of the first peak in cation–anion $g(r)$ for all the systems. Values in Å.

| | Cl | BF4 | PF6 | TFSI |
|-------|-----|-----|-----|------|
| Pyr12 | 4.4 | 5.0 | 5.4 | 5.5 |
| Pyr13 | 4.2 | 5.0 | 5.4 | 5.5 |
| Pyr14 | 4.2 | 4.9 | 5.1 | 5.5 |
| Pyr15 | 4.1 | 4.7 | 5.1 | 5.3 |
| Pyr16 | 4.3 | 4.7 | 5.1 | 5.3 |

Figure 4 presents the coordination number (CN), calculated as the integral over the first peak of the center-of-mass cation–anion $g(r)$, where we can notice that, for the same anion, we had a slight decrease in the CN value with the increase of the cation aliphatic chain. However, the values were very similar considering different anions, except for the systems with Cl. A similar decreasing trend depending on the size of the cation lateral chain was also reported by Nasrabadi and coworkers [63], which suggests that the increase in the alkyl chain decreased the degree of ordering in the ionic liquid.

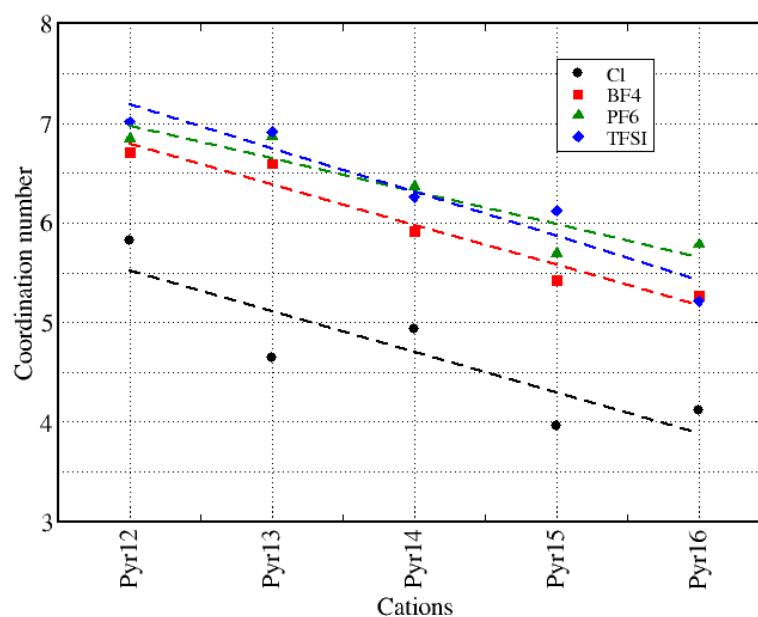


Figure 4. Coordination number (CN) of all neat ionic liquids.

Figure 5 presents the histograms of the number of anions around a cation within a distance of 5 Å, and Figure 6 shows the number of cations around each anion at the same distance, averaged over the entire whole MD trajectory for all systems and using the center-of-mass as a reference. We can observe that, corresponding to the coordination number analysis presented in Figure 4, the figures show similar distributions for all anions, except for Cl. In a more general view, we can see that we have a broader distribution for anions around the cations (Figure 5) than for cations around the anions (Figure 6), which is probably related to the symmetry of the anions. We can also notice that the distributions are similar if we consider different cations around a given anion. It is worth remembering that we intend to discuss in the following sections how these structural properties varied when we replaced different amounts of pyrrolidinium cations with lithium cations.

3.2. Li-Ionic Liquid Electrolyte Solutions

Here, we present the results for the IL–Li-ion electrolyte solutions, with the IL formed by pyrrolidinium cations (Pyr1X: X = 2, . . . , 6), the anions BF₄, PF₆, and TFSI, and replacing fractions of the cations (0.25 and 0.50) by Li with a 1:1 proportion. We discuss the variations of the structural properties such as the density, $g(r)$, and solvation when we compare the systems with and without Li and also present the dynamic properties transference number of Li (t_{Li}) and self-diffusion. Figure 7 shows the density of the ionic liquid–Li electrolyte solutions, in which a fraction of the pyrrolidinium cations were replaced by lithium cations, in comparison with the density of pure ionic liquid systems. As discussed in the previous section, for the neat ionic liquids (0.0 fraction of Li), the density values varied more significantly with the size of the anion than with the size of the cation lateral chain, at least for chains up to six carbon atoms. This trend was preserved when we replaced a fraction of the pyrrolidinium cations by lithium ions. Furthermore, for each ionic liquid, the density values increased as we increased the fraction of Li-ions in the system.

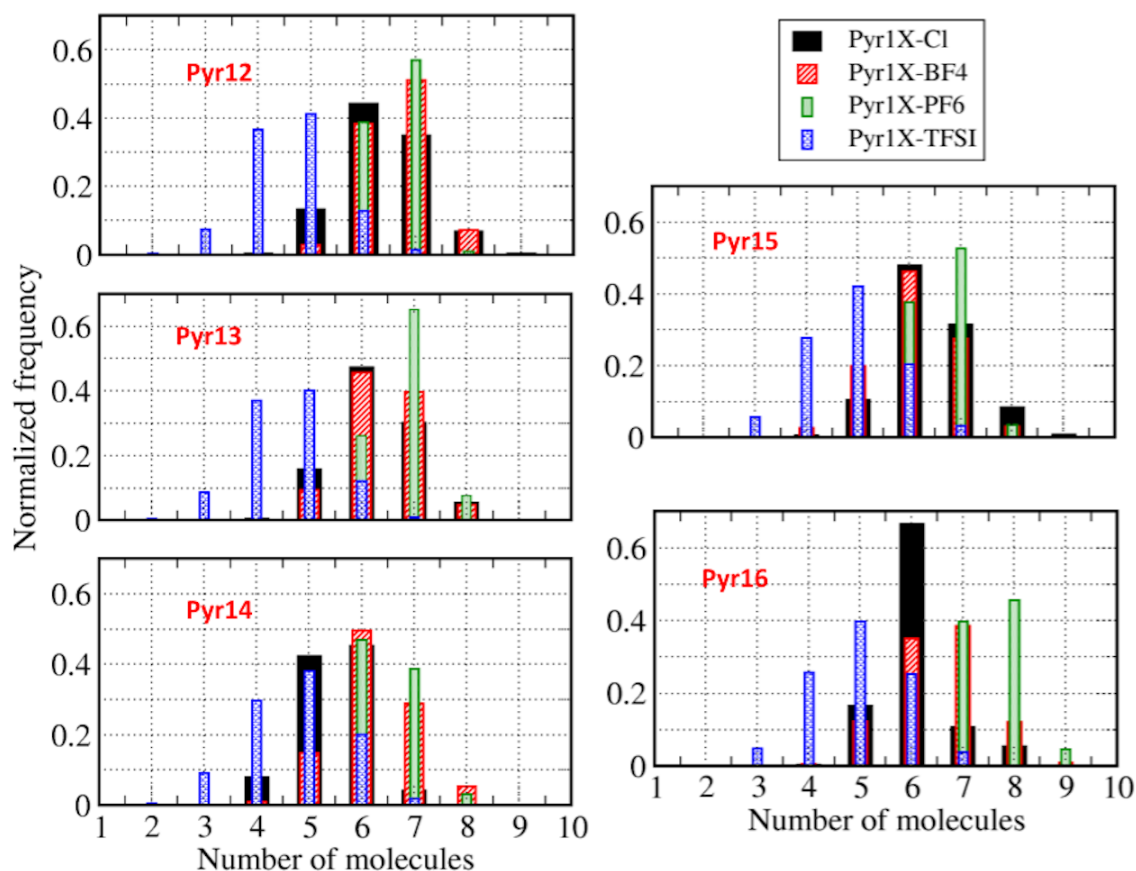


Figure 5. Histograms of the number of anions within 5 Å of one cation.

Figure 8 shows the percentage of the increase in the density with respect to the neat ionic liquids, highlighting that, with the same concentration of Li, the percentage increases in density were similar: for all ionic liquids, the presence of 0.25 Li (\diamond of different colors) led to an increase in the range of 6–8%, while for 0.50 Li (\square of different colors), it was in the range of 13–20%. In this representation, we can see that, in most cases, the variation in density depended on the anion and the cation, and for both fractions of lithium, the systems with PF6 had a larger increase in density compared to the other ILs. This variation in density with the addition of different amounts of lithium is in agreement with what was reported by Mendez-Morales in previous works [9], in which an increase of 5% for smaller amounts of Li and around 12% for 40% of it were reported.

From the analysis of the $g(r)$, we observed that the increase in the amount of lithium practically did not affect the cation–cation $g(r)$, and therefore, it did not affect the cations' structuration. On the other hand, it affected the cation–anion and anion–anion $g(r)$ structuration. For the cation–cation $g(r)$ (Supplementary Material, Figure S4), we can observe that the height of the first peak decreased with the increase in the cation aliphatic chain, and the peak width was smaller for the smaller cations, as happened for the neat ionic liquids. There was also a small dislocation of the first peak to larger r values as the size of the cation, i.e., the size of their aliphatic chains increased. The variation in height of the peaks as the fraction of lithium increased was due to the fact that $g(r)$ was normalized by the density, and except for the height, there was no variation in the curves in systems with BF4 and PF6 with the increase of the Li concentration.

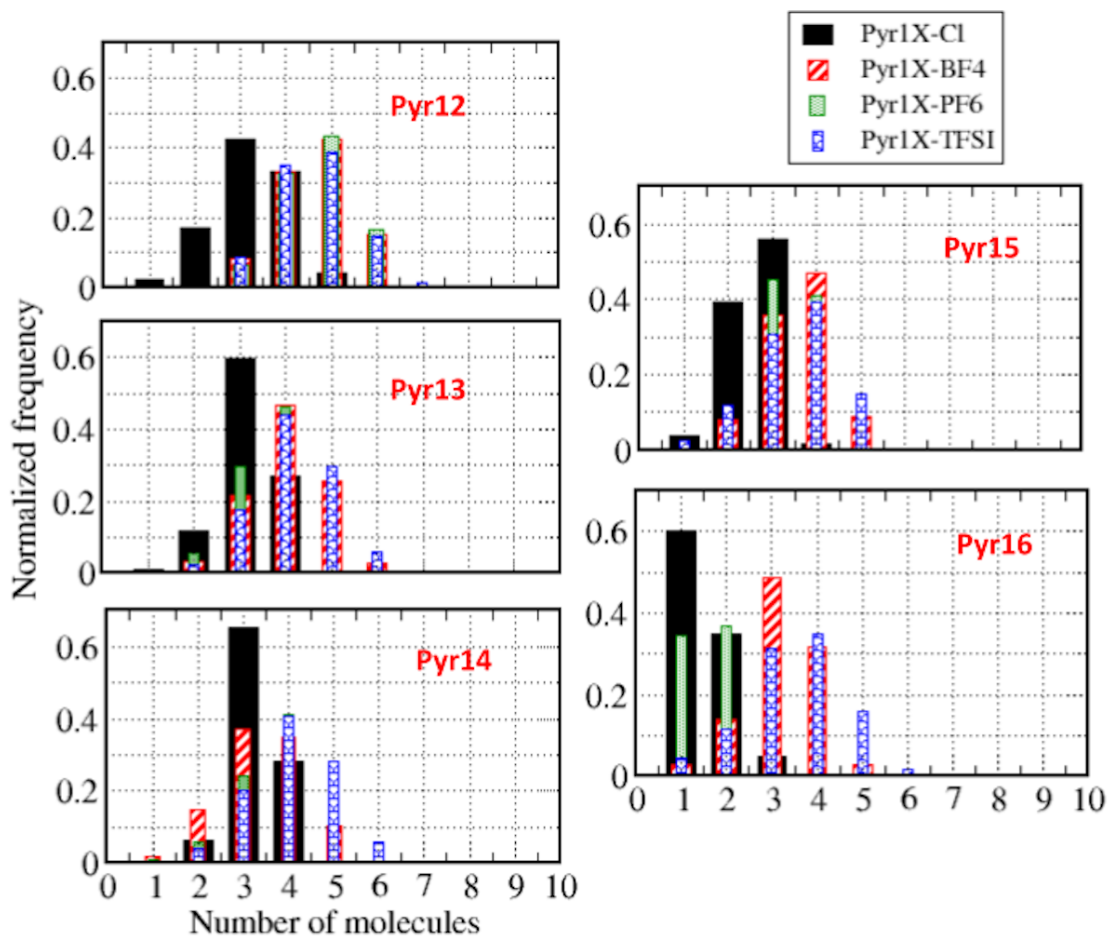


Figure 6. Histograms of the number of cations within 5 Å of one anion.

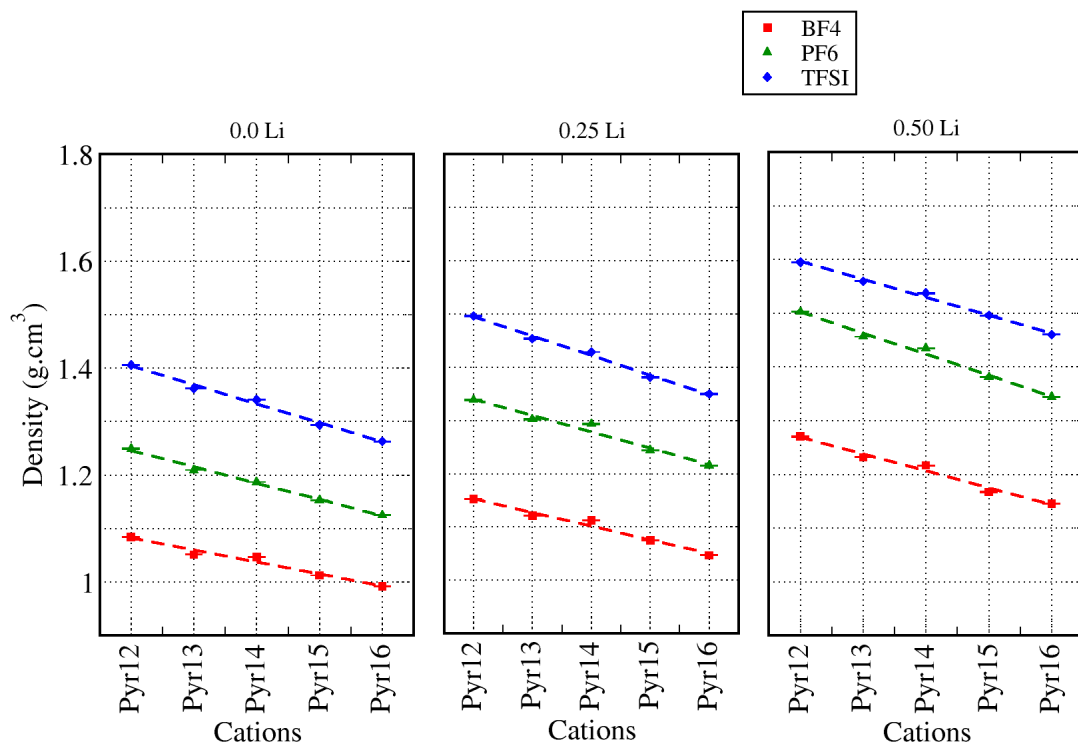


Figure 7. Densities for all systems with different amounts of lithium.

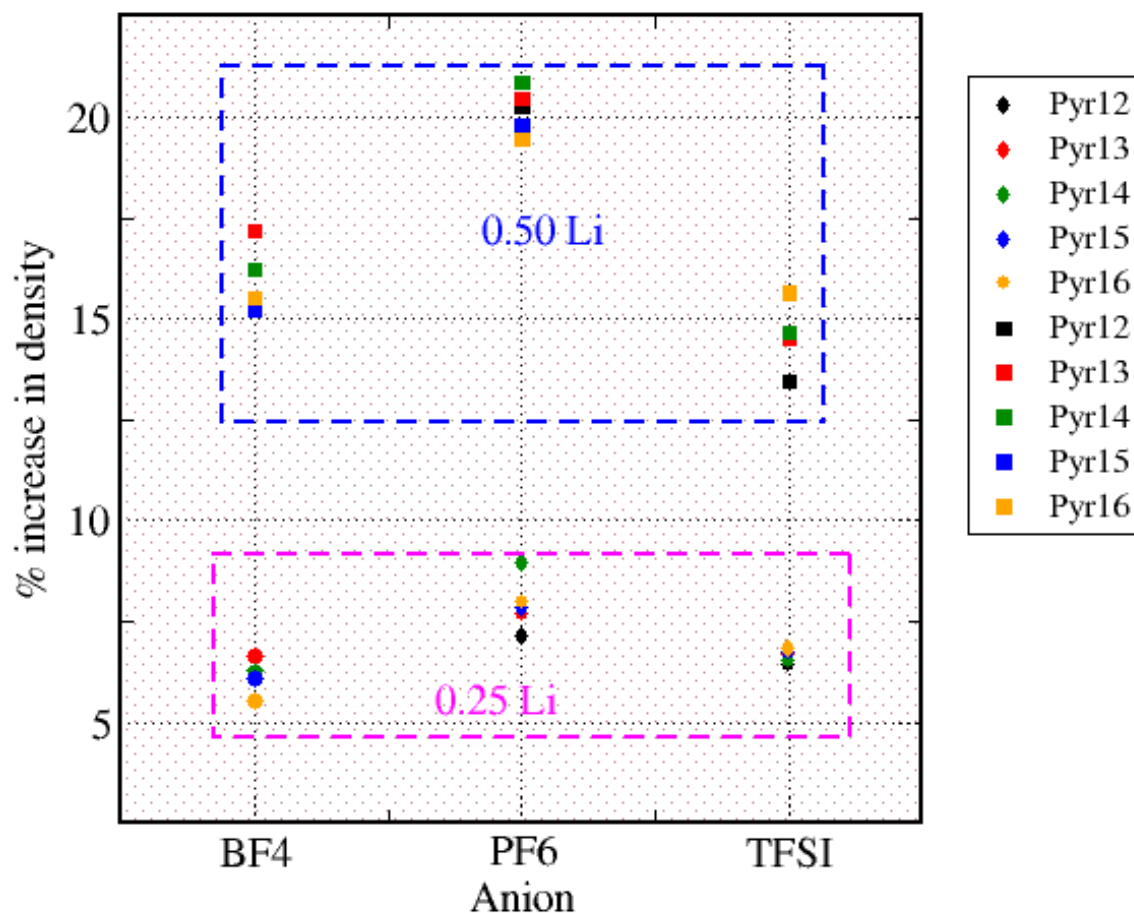


Figure 8. Percentage of the increase in density with respect to the neat ionic liquids.

Figure 9 presents the center-of-mass cation–anion $g(r)$ for the same systems with different amounts of lithium. We can observe that we had a small dislocation of the first peak to smaller values of r as the size of the cation increased. Furthermore, considering systems Pyr1X–BF4 and Pyr1X–PF6, for Pyr16, a second peak appeared very close to the first one, at the same time that the intensity of the peak decreased, which also happened for Pyr15 (Supplementary Material: Figures S5–S7). We can suggest from this that, for the smaller cations, the first solvation shell was more uniform, and for the larger ones, some anions were closer to the cation than others, forming a non-uniform solvation layer, since the anions were symmetric and the cations were not, especially the ones with a longer aliphatic chain. In systems with Pyr1X–TFSI and 0.25 Li, in the case of the larger cations (Pyr16 and Pyr15), there was only one well-defined peak, and a second peak appeared for the cases with the smaller cations (X: 2–3). For Pyr1X–TFSI with 0.50 Li, the second peak decreased as the size of the Pyr1X aliphatic chain decreased, but it was still present for Pyr16.

Figure 10 presents the center-of-mass anion–anion $g(r)$, for the same systems. Different from the other $g(r)$ curves, this $g(r)$ underwent significant changes as the amount of lithium increased. As presented in Supplementary Material Figure S2, Pyr1X–BF4 and Pyr1X–PF6 with no lithium showed a well-defined first peak for all systems and a small shoulder close to it in the systems with smaller cations, forming a double-peak structure, which suggests two preferred positions or orientations of the anions. There was also in this case a small dislocation of the position of the first peak to larger r values, as happened for cation–cation $g(r)$, and this dislocation was less significant for systems with TFSI. Furthermore, for TFSI, there was never the double peak.

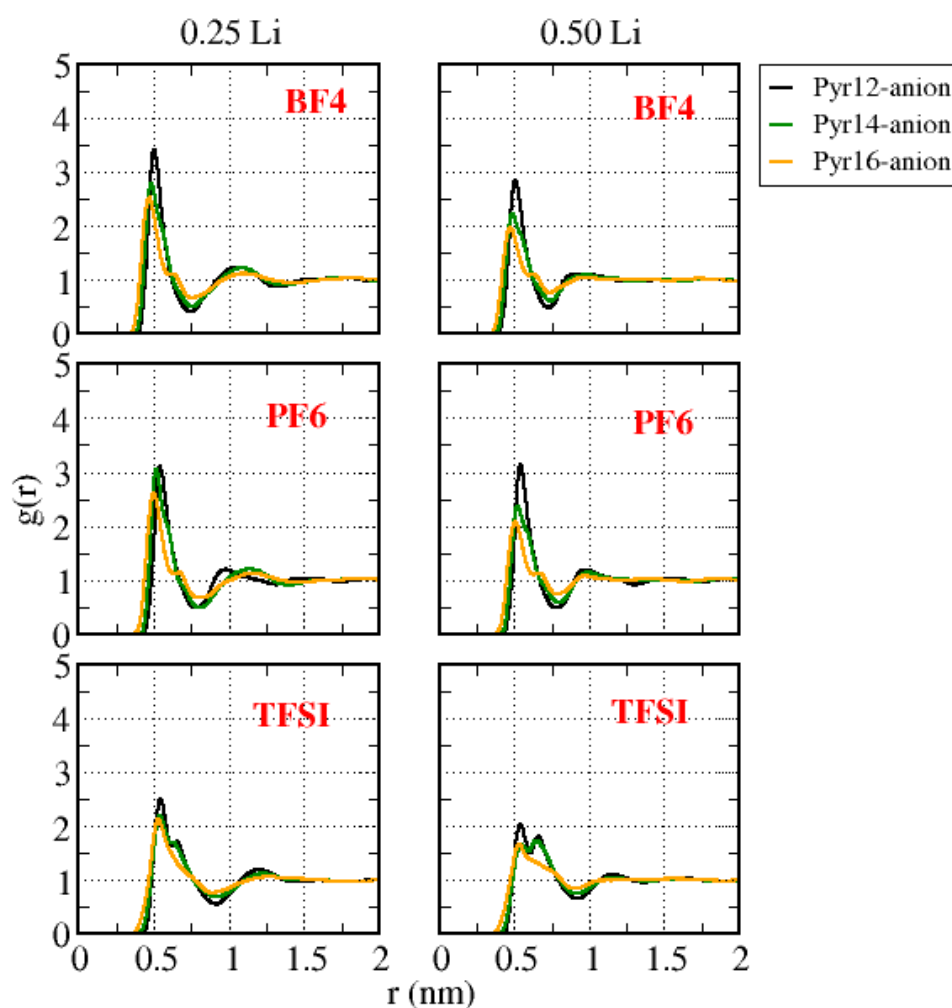


Figure 9. Center-of-mass cation–anion $g(r)$ for all the systems with different amounts of lithium.

The substitution of Pyr with Li strongly altered the form of the curves: systems with Pyr1X–BF4 presented a double first peak in all cases instead of the well-defined first peak in the systems without Li, as well as a double second peak at a 0.25 Li concentration with small cations. Systems with Pyr1X–PF6 presented a well-defined first peak, but a second small peak arose in all cases, with different forms and positions depending on the cation and on the Li content. TFSI-based ILs with 0.25 Li presented a small double peak, the second one being higher than the first one, and with 0.50 Li, a higher first peak. A similar trend was observed by Haskins and co-workers [32]. The peak located at larger r corresponded to the anions that were strongly bound to Li, while the peak at smaller r corresponded to the anions coordinated to the pyrrolidinium cations, suggesting that increasing the amount of Li, the average anion–anion distance increased.

Figure 11 shows the center-of-mass Li–anion $g(r)$ for all the systems with lithium. We can notice that the intensity and the form of the peaks were different for different anions. These intensities could allow one to infer the strength of the Li-ion interactions, noticing that Li–BF4 was the stronger one, followed by Li–TFSI and Li–PF6, respectively. Furthermore, if we considered the end of the first peak as the end of the first solvation shell (0.35 nm for BF4, 0.40 nm for PF6, and 0.50 nm for TFSI), all systems presented a double peak, indicating that the Li-ions coordinated with more than one anion. The length of the aliphatic chain of pyrrolidinium ions did not affect either the position or the form of the peak in $g(r)$, except for the systems with PF6 as the anion and a 0.25 Li fraction.

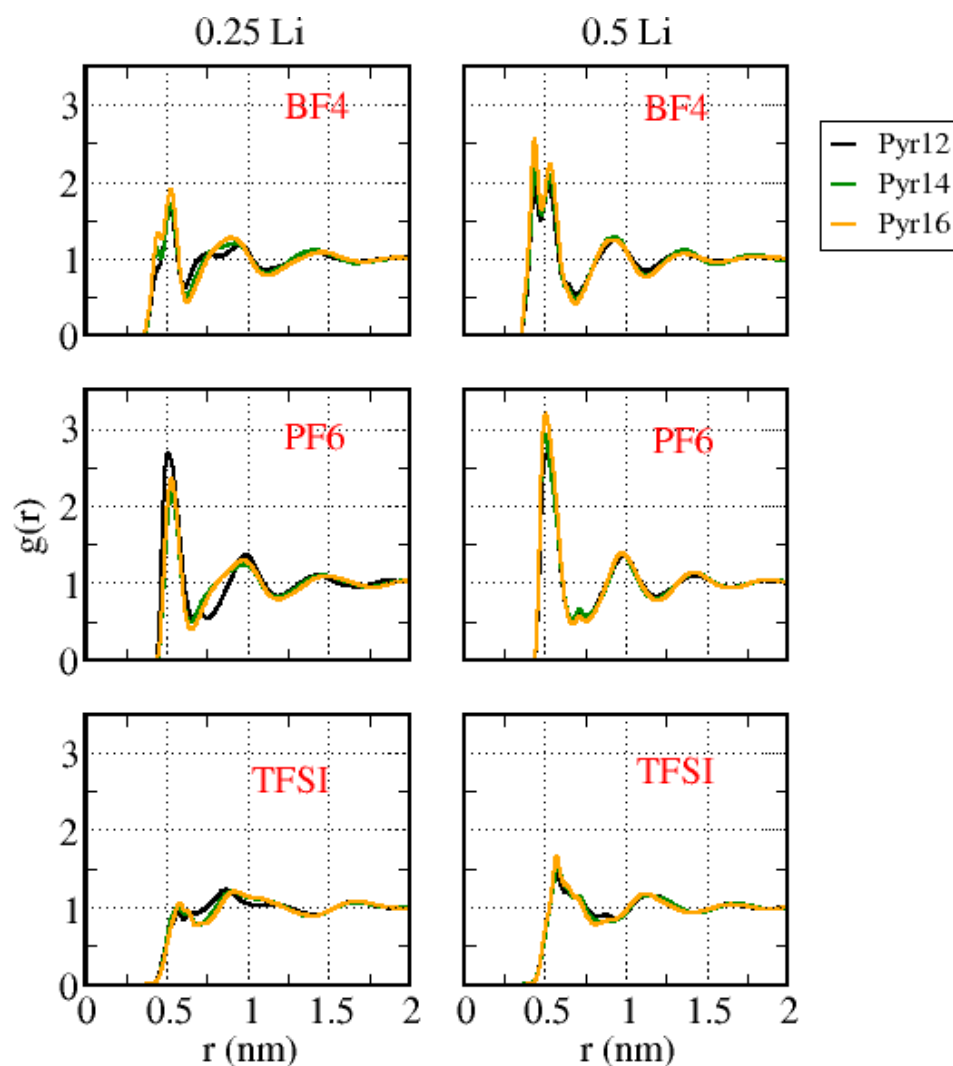


Figure 10. Center-of-mass anion–anion $g(r)$ for all the systems with different amounts of lithium.

Based on the results of $g(r)$, we propose a strategy to understand how the ions aggregate in the system: considering the Li–anion distance (r) obtained from $g(r)$, we used a Gromacs tool to select all Li cations in the box and to count how many anions there were at a distance r of those Li-ions, then divided by the number of Li-ions in the system, along the trajectory. From this result, we built the histograms shown in Figure 12, (a) for systems with 0.25 Li and (b) with 0.50 Li. From these results, we can observe that, in Pyr1X–BF4: 0.25 Li, the Li-ions were on average close to more than two anions. Systems with PF6 as the anion had a non-linear behavior: with Pyr13 and Pyr14, Li was close to less than 2 anions, and with Pyr12, Pyr15, and Pyr16, Li was close to more than 2 anions. Finally, systems with TFSI as the anion had only one TFSI close to each Li in most cases, the exception being the system with Pyr14–TFSI. Therefore, we suggest that Li-ions form clusters with the anions, which reduces their mobility, as happens in systems with imidazolium-based ionic liquids combined with the same anions and different amounts of lithium [8,9].

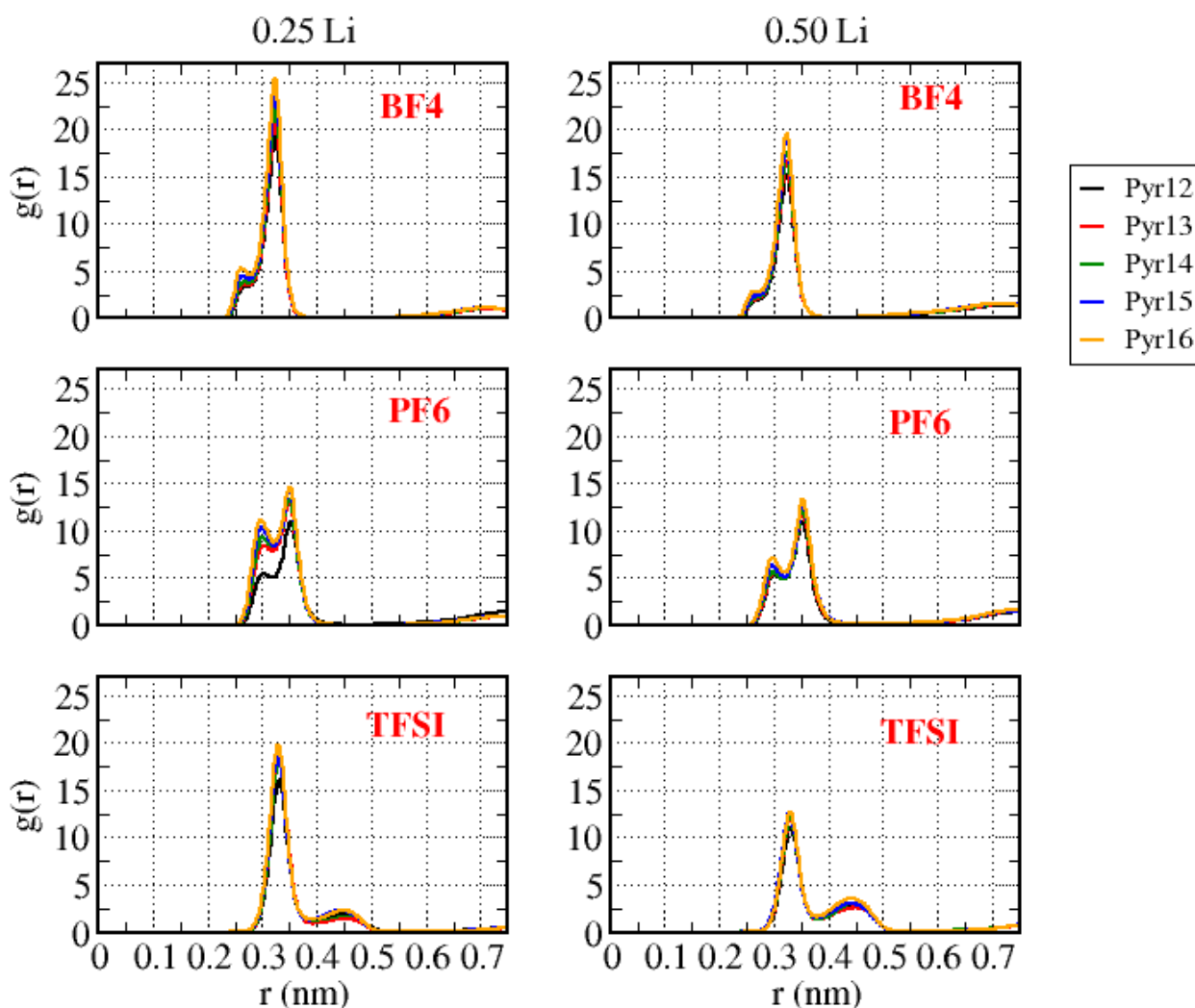
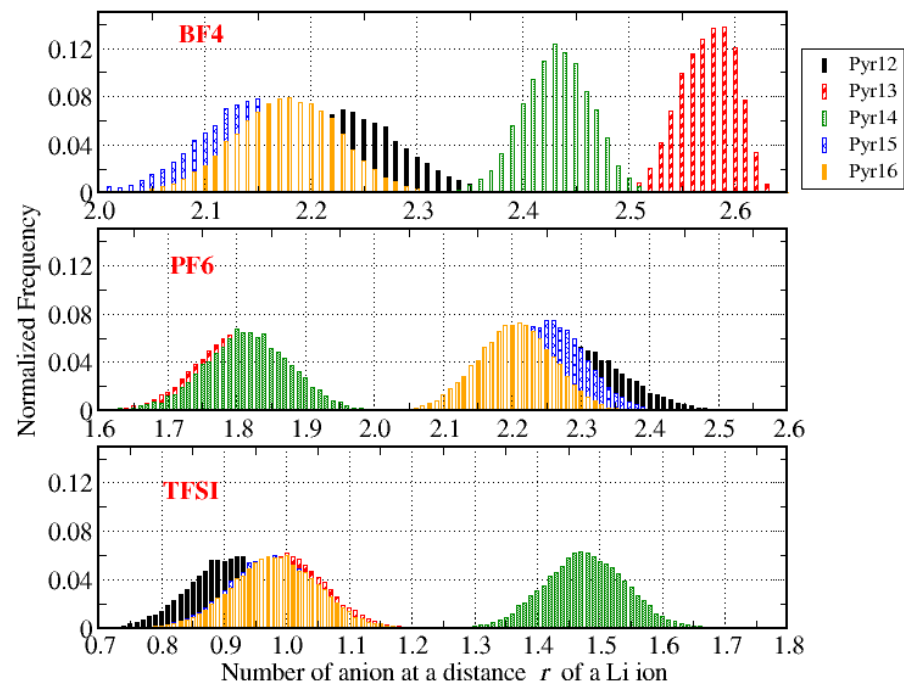


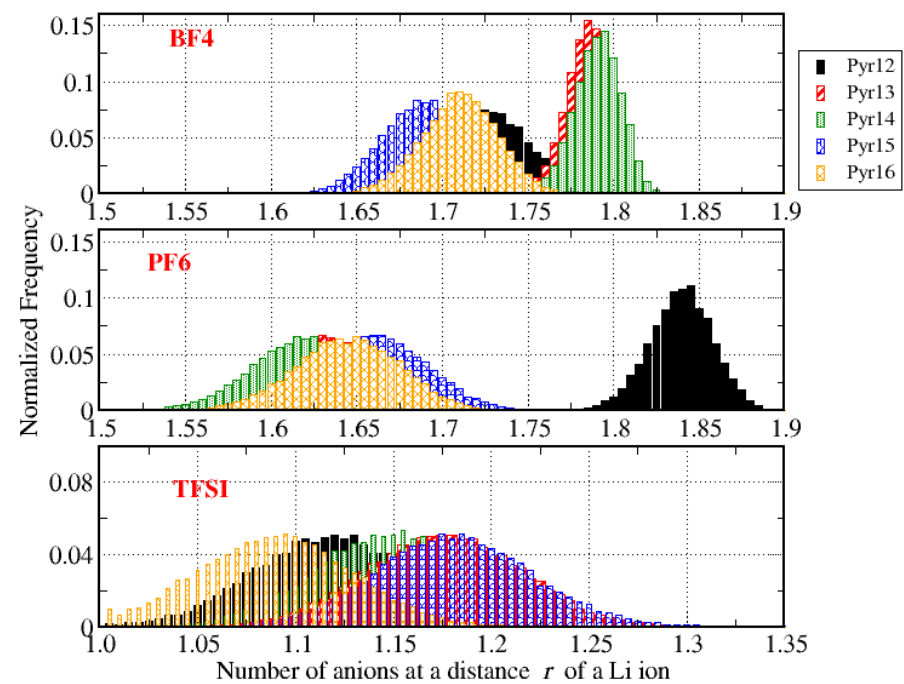
Figure 11. Center-of-mass Li-anion $g(r)$ for all the systems with different amounts of lithium.

Systems with a larger fraction of lithium (0.50 Li) had a similar trend depending on the size of the pyrrolidinium cation for systems with BF₄ and PF₆ as the anions, considering that the average number of anions around the lithium ions was in the range 1.5–2.0, while for TFSI as the anion, the average was close to 1.0 for the systems. For all systems with TFSI in this case, there would be no “free” lithium, in the sense that all distributions in the histograms were larger than 1, so apparently increasing the fraction of lithium, the amount of “free” lithium decreased, although we would expect the opposite trend.

If we look at the average number of anions around one Li, we can see that systems with PF₆ and BF₄ anions and 0.25 Li formed larger clusters, and this average number varied for Pyr1X cations with different side chains (different X) in an unclear trend. Indeed, for 0.25 Li, Pyr13–BF₄ and Pyr14–BF₄ seemed on average to form larger clusters than Pyr13–PF₆ and Pyr14–PF₆, while the other cations showed the same cluster size, independent of the anion. The Pyr1X–TFSI systems formed clusters involving more than one TFSI with lithium only in the system with Pyr14. For 0.50 Li, the trend was clearer: PF₆ and BF₄ formed clusters with more than one lithium, and TFSI coordinated with one lithium.



(a)



(b)

Figure 12. Histograms of the number of anions around the Li-ions throughout the trajectories, for all systems. In (a) with 0.25 Li and in (b) with 0.50 Li.

Considering the systems Pyr12–TFSI, Pyr13–TFSI, Pyr15–TFSI, and Pyr16–TFSI, all with 0.25 Li, that had the average number of anions around the Li smaller than 1, if we

assumed that we can have up to 3 anions that could be “free” throughout the trajectory, we can calculate the degree of dissociation (α), defined as

$$\alpha = \frac{N_{Li}}{N_{Li-anion}} \quad (3)$$

where N_{Li} is the number of “free” Li-ions and $N_{Li-anion}$ is the total number of Li-ions forming Li-anion ionic pairs. Therefore, we had for all these cases $\alpha = 0.03$ [69].

3.3. Dynamical Properties

As mentioned previously, the self-diffusion of the ionic species was obtained from mean-squared displacement (MSD) calculations. These results are presented in Figure 13. The first thing to mention is that, in systems with no lithium, both species self-diffused faster than in the systems with lithium, i.e., the self-diffusion of the species invariably decreased as the amount of lithium increased, and in systems with BF₄ and TFSI, the cations diffused faster than the anions. On the other hand, for systems with 0.25 Li and TFSI as the anion, all species diffused faster. It has been reported in the literature that the diffusion of lithium is usually smaller by one order of magnitude than the diffusion of the other ionic species, especially because Li tends to be strongly bonded to the anions, as well as because the density increases with the increase of the lithium fraction. Considering the diffusion of Li in each system, if one has to choose one among the ionic liquids presented here for an application that requires a better self-diffusion, it seems more interesting to use Pyr13–BF₄, Pyr15–BF₄, Pyr16–BF₄, Pyr13–TFSI, and Pyr14–TFSI, all with 0.25 Li. The general trend of Li diffusion following this order TFSI > BF₄ > PF₆ is coherent with other studies reported [9].

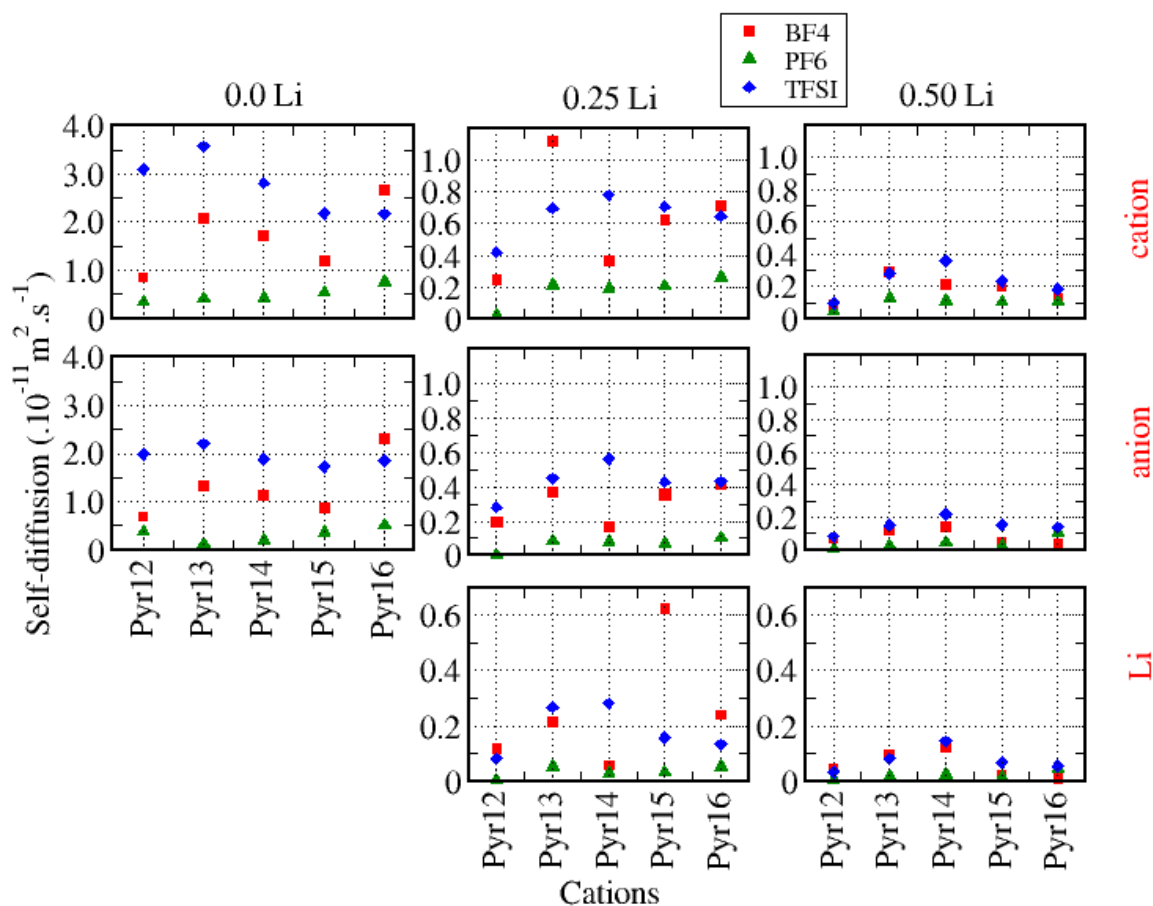


Figure 13. Self-diffusion of all species in the systems considered.

As explained in Section 2, from the self-diffusion values of all species, we can calculate the transference number (Equation (2)). Figure 14 presents the Li transference number (t_{Li}) as a function of Pyr1X, for the systems with different amounts of lithium. It has been reported in literature [26,64] that t_{Li} normally increases with the lithium fraction, but for some cases, there is a competition between the effect of increasing the lithium fraction and the increment in viscosity due to it. Lourenço and co-workers [64] also suggested that t_{Li} is mainly ruled by viscosity and Li–anion interaction. The systems that had BF₄ as the anion did not show a clear trend either with the variation of the cations or with the amount of lithium: for smaller cations (Pyr12, Pyr13, and Pyr14), t_{Li} increased linearly with the cation size in each Li fraction and increased significantly with the increase in the lithium fraction. For Pyr15, t_{Li} was larger for 0.25 Li, while for Pyr16, it was larger for 0.50 Li. Systems with PF₆ as the anion showed a clear increase in t_{Li} with the increase in the Li fraction except for Pyr16, and with the variation of t_{Li} for systems with TFSI, the trend depending on the cation size was very similar for both Li fractions. Based on these results, a larger fraction of lithium would allow the use of different combinations of cations and anions to improve the performance.

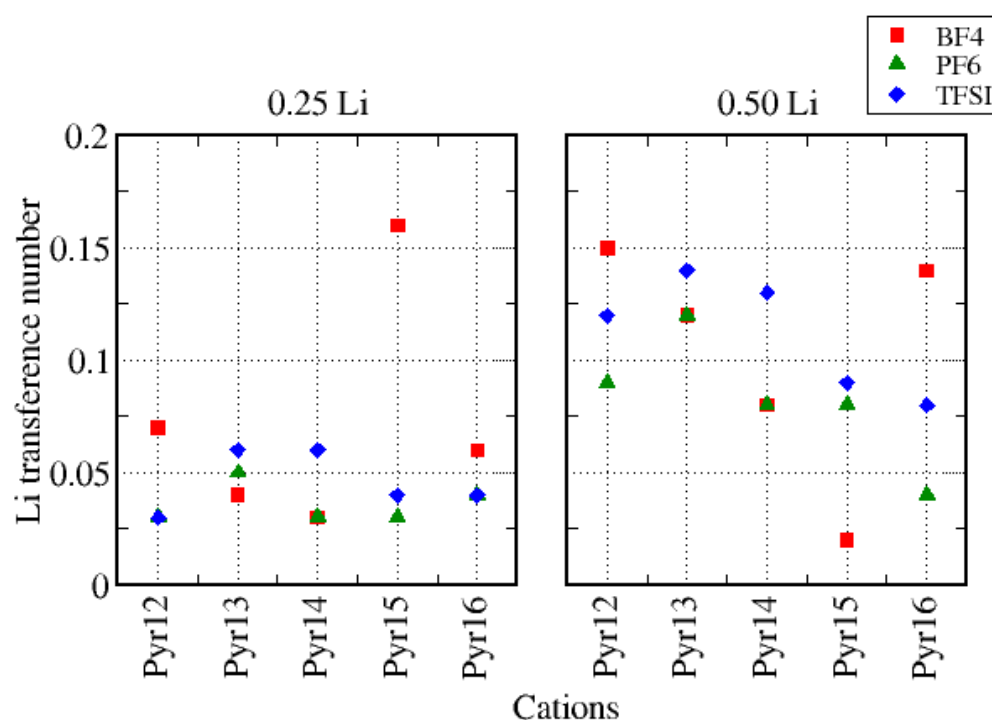


Figure 14. Transference number (t_{Li}) as a function of Pyr1X, for the systems with different amounts of lithium.

4. Conclusions

In this work, we used molecular dynamics simulations to systematically study the properties of neat ionic liquids formed by pyrrolidinium cations with different sizes of aliphatic chains and anions with different sizes, shapes, and symmetry profiles, from the monoatomic Cl[−] to the bulky TFSI. We investigated how structural properties such as the density, pair correlation function, and solvation determine the self-organization of these species. Based on this broad view, we analyzed how these properties varied as we replaced a fraction of the pyrrolidinium cations by lithium ions, forming a ternary solution. Finally, we evaluated how the structural parameters, together with dynamic properties such as self-diffusion and transference number, could determine the more appropriate cation–anion combinations and lithium fraction, which will support the use of Li-ion batteries.

We observed that neat ionic liquids presented a density value that increased significantly as we increased the anion size and slightly increased as we increased the cation

aliphatic chain. This trend was preserved when we replaced part of the pyrrolidinium cations by lithium cations; however, the larger the Li fraction, also the greater was the density. The $g(r)$ curves underwent more significant changes in shape and first peak position when the kind of anion was changed than when the cations or lithium amounts were changed. The cation–anion and anion–anion $g(r)$ curves presented differences with the increase of Li, showing in some cases shoulders slightly before or after the first peak, showing more than one preferential position for the ions in the solvation shell.

From the analysis of the dissociation degree, we propose that 0.25 Li–Pyr1X–TFSI systems, except 0.25 Li–Pyr14–TFSI, could be good for applications in Li-ion batteries, since these dissociated ions could move more easily in the electrolyte solution. On the other hand, the Li self-diffusion analysis showed a similar trend for TFSI, with Pyr13 and Pyr14 as the most-promising cations. The transference number results also pointed out TFSI as the most-promising anion, also for larger concentrations of Li.

Our analyses showed that Li-ions usually form clusters with more than one anion, but for the TFSI-based ILs, where Li usually “bonds” to only one anion. The number of molecules on the Li solvation shell depends both on the specific cation–anion combination and on the Li fraction in the solution. Therefore, we can propose that large amounts of lithium do not necessarily increase the Li-ion mobility, because more clusters can be formed, which will tend to decrease the lithium mobility.

Supplementary Materials: The following supporting information can be downloaded at: <https://www.mdpi.com/article/10.3390/batteries9040234/s1>, Table S1: Identification of all species considered in this paper; Table S2: Energy values obtained from DFT calculations of each species; Figure S1: Calculated molar mass of cations and anions; Figure S2: Center-of-mass cation-cation, cation-anion and anion-anion pair correlation functions ($g(r)$); Figure S3: Center-of-mass cation-cation, cation-anion and anion-anion pair correlation functions ($g(r)$); Figure S4: Center-of-mass cation-cation $g(r)$ with all fractions of Li; Figure S5: Center-of-mass cation-anion $g(r)$ with all fractions of Li; Figure S6: Center-of-mass anion-anion $g(r)$ with all fractions of Li; Figure S7: Center-of-mass cation-cation $g(r)$ for systems Pyr12-anion, Pyr14-anion and Pyr16-anions.

Author Contributions: Conceptualization, M.A.S., R.M. (Rita Maji), E.D., A.R. and R.M. (Rita Magri); formal analysis, M.A.S., E.D., A.R. and R.M. (Rita Magri); investigation, M.A.S. and R.M. (Rita Maji); methodology, M.A.S. and R.M. (Rita Maji); project administration, R.M. (Rita Magri); resources, R.M. (Rita Magri); supervision, E.D., A.R. and R.M. (Rita Magri); visualization, M.A.S., R.M. (Rita Maji) and F.R.; writing—original draft, M.A.S. and R.M. (Rita Maji); writing—review and editing, M.A.S., R.M. (Rita Maji), F.R., E.D., A.R. and R.M. (Rita Magri). All authors have read and agreed to the published version of the manuscript.

Funding: This research was developed under the framework of the BAT4EVER project, which has received funding from the European Union’s Horizon 2020 research and innovation program under Grant Agreement No 957225. This project was partially funded under the National Recovery and Resilience Plan (NRRP), Mission 04 Component 2 (a) Investment 1.5—Next Generation EU, Call for Tender No. 3277, dated 30 December 2021. Award Number: 0001052 dated 23 June 2022 (F. Rossella, A. Ruini, E. Degoli, and R. Magri), and (b) Investment 1.4 e D.D. 1033 dated 17 June 2022, CN00000023 (E. Degoli and R. Magri). This manuscript reflects only the authors’ views and opinions; neither the European Union, nor the European Commission can be considered responsible for them.

Data Availability Statement: Not applicable.

Acknowledgments: M. Salvador would like to thank the University of Modena and Reggio Emilia for the financial support and HPC facilities. We would also like to acknowledge the CINECA HPC facility for the approved ISCR A (IscrA_POLYFACE) and ISCR B projects (IscrB_Interpol, IscrB_SEE-NOW, IscrB_PEs-LiMD, IscrB_PaniLiB).

Conflicts of Interest: The authors declare no conflict of interest.

References

1. Thum, A.; Heuer, A.; Shimizu, K.; Canongia Lopes, J.N. Solvate ionic liquids based on lithium bis(trifluoromethanesulfonyl)imide-glyme systems: Coordination in MD simulations with scaled charges. *Phys. Chem. Chem. Phys.* **2020**, *22*, 525–535. [[CrossRef](#)] [[PubMed](#)]
2. Borodin, O. Polarizable Force Field Development and Molecular Dynamics Simulations of Ionic Liquids. *J. Phys. Chem. B* **2009**, *113*, 11463–11478. [[CrossRef](#)] [[PubMed](#)]
3. Paredes, X.; Fernández, J.; Pádua, A.A.H.; Malfreyt, P.; Malberg, F.; Kirchner, B.; Pensado, A.S. Bulk and Liquid-Vapor Interface of Pyrrolidinium-Based Ionic Liquids: A Molecular Simulation Study. *J. Phys. Chem. B* **2014**, *118*, 731–742. [[CrossRef](#)] [[PubMed](#)]
4. Choi, J.A.; Sun, Y.K.; Shim, E.G.; Scrosati, B.; Kim, D.W. Effect of 1-butyl-1-methylpyrrolidinium hexafluorophosphate as a flame-retarding additive on the cycling performance and thermal properties of lithium-ion batteries. *Electrochim. Acta* **2011**, *56*, 10179–10184. [[CrossRef](#)]
5. Tiago, G.A.O.; Matias, I.A.S.; Ribeiro, A.P.C.; Martins, L.M.D.R.S. Application of Ionic Liquids in Electrochemistry—Recent Advances. *Molecules* **2020**, *25*, 5812. [[CrossRef](#)] [[PubMed](#)]
6. Farahipour, R.; Mehrkesh, A.; Karunanithi, A.T. A systematic screening methodology towards exploration of ionic liquids for CO₂ capture processes. *Chem. Engin. Sci.* **2016**, *145*, 126–132. [[CrossRef](#)]
7. Gnezdilov, O.I.; Filippov, A.; Khan, I.A.; Shah, F.U. Translational and reorientational dynamics of ionic liquid-based fluorine-free lithium-ion battery electrolytes. *J. Mol. Liq.* **2022**, *345*, 117001. [[CrossRef](#)]
8. Judeinstein, P.; Zeghal, M.; Constantin, D.; Ioioiu, C.; Coasne, B. Interplay of Structure and Dynamics in Lithium/Ionic Liquid Electrolytes: Experiment and Molecular Simulation. *J. Phys. Chem. B* **2021**, *125*, 1618–1631. [[CrossRef](#)]
9. Méndez-Morales, T.; Carrete, J.; Bouzón-Capelo, S.; Pérez-Rodríguez, M.; Cabeza, O.; Gallego, L.J.; Varela, L.M. MD Simulations of the Formation of Stable Clusters in Mixtures of Alkaline Salts and Imidazolium-Based Ionic Liquids. *J. Phys. Chem. B* **2013**, *117*, 3207–3220. [[CrossRef](#)]
10. Ray, P.; Vogl, T.; Balducci, A.; Kirchner, B. Structural Investigations on Lithium-Doped Protic and Aprotic Ionic Liquids. *J. Phys. Chem. B* **2017**, *121*, 5279–5292. [[CrossRef](#)] [[PubMed](#)]
11. Sánchez, L.G.; Espel, J.R.; Onick, F.; Meindersma, G.W.; Haan, A.B. Density, Viscosity, and Surface Tension of Synthesis Grade Imidazolium, Pyridinium, and Pyrrolidinium Based Room Temperature Ionic Liquids. *J. Chem. Eng. Data* **2009**, *54*, 2803–2812. [[CrossRef](#)]
12. Kunze, M.; Jeong, S.; Paillard, E.; Winter, M.; Passerini, S. Melting Behavior of Pyrrolidinium Based Ionic Liquids and Their Binary Mixtures. *J. Phys. Chem. C* **2010**, *114*, 12364–12369. [[CrossRef](#)]
13. Brutti, S. Pyr_{1,x}-TFSI Ionic Liquids (x = 1–8): A Computational Chemistry Study. *Appl. Sci.* **2020**, *10*, 8552. [[CrossRef](#)]
14. Molinari, N.; Mailoa, J.P.; Kozinsky, B. General Trend of a Negative Li Effective Charge in Ionic Liquid Electrolytes. *J. Phys. Chem. Lett.* **2019**, *10*, 2313–2319. [[CrossRef](#)]
15. Postupna, O.O.; Kolesnik, Y.V.; Kalugin, O.N.; Prezhdo, O.V. Microscopic Structure and Dynamics of LiBF₄ Solutions in Cyclic and Linear Carbonates. *J. Phys. Chem. B* **2011**, *115*, 14563–14571. [[CrossRef](#)]
16. Pires, J.; Timperman, L.; Jacquemin, J.; Balducci, A.; Anouti, M. Density, conductivity, viscosity, and excess properties of (pyrrolidinium nitrate-based Protic Ionic Liquid + propylene carbonate) binary mixture. *J. Chem. Thermodyn.* **2013**, *59*, 10–19. [[CrossRef](#)]
17. Xiao, W.; Yang, Q.; Zhu, S. Comparing ion transport in ionic liquids and polymerized ionic liquids. *Sci. Rep.* **2020**, *10*, 7825–7837. [[CrossRef](#)]
18. Sharma, S.; Kashyap, H.K. Interfacial Structure of Pyrrolidinium Cation Based Ionic Liquids at Charged Carbon Electrodes: The Role of Linear and Nonlinear Alkyl Tails. *J. Phys. Chem. C* **2017**, *121*, 13202–13210. [[CrossRef](#)]
19. Philippi, F.; Welton, T. Targeted modifications in ionic liquids—From understanding to design. *Phys. Chem. Chem. Phys.* **2021**, *23*, 6993–7021. [[CrossRef](#)]
20. MacGrath, L.M.; Rohan, J.F. Pyrrolidinium Containing Ionic Liquid Electrolytes for Li-Based Batteries. *Molecules* **2020**, *25*, 6002. [[CrossRef](#)]
21. Murugesan, S.; Quintero, O.A.; Chou, B.P.; Xiao, P.; Park, K.; Hall, J.W.; Jones, R.A.; Henkelman, G.; Goodenough, J.B.; Stevenson, K.J. Wide electrochemical window ionic salt for use in electropositive metal electrodeposition and solid state Li-ion batteries. *J. Mater. Chem. A* **2014**, *2*, 1294–1302. [[CrossRef](#)]
22. Ray, A.; Saruhan, B. Application of Ionic Liquids for Batteries and Supercapacitors. *Materials* **2021**, *14*, 2942. [[CrossRef](#)]
23. Hayamizu, K.; Tsuzuki, S.; Seki, S.; Fujii, K.; Suenaga, M.; Umebayashi, Y. Studies on the translational and rotational motions of ionic liquids composed of N-methyl-N-propyl-pyrrolidinium (P₁₃) cation and bis(trifluoromethanesulfonyl)amide and bis(fluorosulfonyl)amide anions and their binary systems including lithium salts. *J. Chem. Phys.* **2010**, *133*, 194505. [[CrossRef](#)]
24. Celeste, A.; Silvestri, L.; Agostini, M.; Sadd, M.; Palumbo, S.; Panda, J.K.; Matic, A.; Pellegrini, V.; Brutti, S. Enhancement of Functional Properties of Liquid Electrolytes for Lithium-Ion Batteries by Addition of Pyrrolidinium-Based Ionic Liquids with Long Alkyl-Chains. *Batter. Supercaps* **2020**, *3*, 1059–1068. [[CrossRef](#)]
25. Al-Rashed, O.A.; Nazzar, A.A. Ionic liquids with superior protection for mild steel in acidic media: Effects of anion, cation, and alkyl chain length. *J. Mol. Liquids* **2019**, *288*, 111015–111026. [[CrossRef](#)]
26. Lesch, V.; Heuer, A.; Holm, C.; Smiatek, J. Properties of Apolar Solutes in Alkyl Imidazolium-Based Ionic Liquids: The Importance of Local Interactions. *ChemPhysChem* **2016**, *17*, 387–394. [[CrossRef](#)]

27. Ray, P.; Balducci, A.; Kirchner, B. Molecular Dynamics Simulations of Lithium-Doped Ionic-Liquid Electrolytes. *J. Phys. Chem. B* **2018**, *122*, 10535–10547. [[CrossRef](#)]
28. Méndez-Morales, T.; Carrete, J.S.; Pérez-Rodríguez, M.; Cabeza, O.; Gallego, L.J.; Lynden-Bell, R.M.; Varela, L.M. Molecular dynamics simulations of the structure of the graphene-ionic liquid/alkali salt mixtures interface. *Phys. Chem. Chem. Phys.* **2014**, *16*, 13271–13278. [[CrossRef](#)]
29. Liu, H.; Maginn, E. Effect of ion structure on conductivity in lithium-doped ionic liquid electrolytes: A molecular dynamics study. *J. Chem. Phys.* **2013**, *139*, 114508. [[CrossRef](#)]
30. Huang, J. Confinement Induced Dilution: Electrostatic Screening Length Anomaly in Concentrated Electrolytes in Confined Space. *J. Phys. Chem. C* **2018**, *122*, 3428–3433. [[CrossRef](#)]
31. Lesch, V.; Li, Z.; Bedrov, D.; Borodin, O.; Heuer, A. The influence of cations on lithium ion coordination and transport in ionic liquid electrolytes: A MD simulation study. *Phys. Chem. Chem. Phys.* **2016**, *18*, 382–393. [[CrossRef](#)]
32. Haskins, J.B.; Bennett, W.R.; Wu, J.J.; Hernández, D.M.; Borodin, O.; Momk, J.D.; Bauschlincher, C.W., Jr.; Lawson, J.W. Computational and Experimental Investigation of Li-Doped Ionic Liquid Electrolytes: [pyr14][TFSI], [pyr13][FSI], and [EMIM][BF₄]. *J. Phys. Chem. B* **2014**, *118*, 11295–11309. [[CrossRef](#)]
33. Rütger, T.; Bhatt, A.I.; Best, A.S.; Harris, K.R.; Hollenkamp, A.F. Electrolytes for Lithium (Sodium) Batteries Based on Ionic Liquids: Highlighting the Key Role Played by the Anion. *Batter. Supercaps* **2020**, *3*, 793–827. [[CrossRef](#)]
34. Seo, D.M.; Boyle, P.D.; Allen, J.L.; Han, S.D.; Jónsson, E.; Johansson, P.; Henderson, W.A. Solvate Structures and Computational/Spectroscopic Characterization of LiBF₄ Electrolytes. *J. Phys. Chem. C* **2014**, *118*, 18377–18386. [[CrossRef](#)]
35. Canongia Lopes, J.N.; Deschamps, J.; Pádua, A.A.H. Modeling Ionic Liquids Using a Systematic All-Atom Force Field. *J. Phys. Chem. B* **2004**, *108*, 2038–2047. [[CrossRef](#)]
36. Jorgensen, W.L.; Maxwell, D.S.; Tirado-Rives, J. Development and Testing of the OPLS All-Atom Force Field on Conformational Energetics and Properties of Organic Liquids. *J. Am. Chem. Soc.* **1996**, *118*, 11225–11236. [[CrossRef](#)]
37. Ponder, J.W.; Case, D.A. Force fields for protein simulations. *Adv. Prot. Chem.* **2003**, *66*, 27–85.
38. Canongia Lopes, J.N.; Pádua, A.A.H. Nanostructural Organization in Ionic Liquids. *J. Phys. Chem. B* **2006**, *110*, 3330–3335. [[CrossRef](#)]
39. Canongia Lopes, J.N.; Shimizu, K.; Pádua, A.A.H.; Umebayashi, Y.; Fukuda, S.; Fujii, K.; Ishiguro, S. A Tale of Two Ions: The Conformational Landscapes of Bis(trifluoromethanesulfonyl)amide and N,N-Dialkylpyrrolidinium. *J. Phys. Chem. B* **2008**, *112*, 1465–1472. [[CrossRef](#)]
40. Canongia Lopes, J.N.; Pádua, A.A.H. CL&P: A generic and systematic force field for ionic liquids modeling. *Theor. Chem. Acc.* **2012**, *131*, 1129–1140.
41. Chen, M.; Pendrill, R.; Widmalm, G.; Brady, J.W.; Wohlert, J. Molecular Dynamics Simulations of the Ionic Liquid 1-n-Butyl-3-Methylimidazolium Chloride and Its Binary Mixtures with Ethanol. *J. Chem. Theory Comput.* **2014**, *10*, 4465–4479. [[CrossRef](#)]
42. McDaniel, J.G.; Choi, E.; Son, C.Y.; Schmidt, J.R.; Yethiraj, A. Ab Initio Force Fields for Imidazolium-Based Ionic Liquids. *J. Phys. Chem. B* **2016**, *120*, 7024–7036. [[CrossRef](#)]
43. Köderman, T.; Paschek, D.; Ludwig, R. Ionic Liquids: Dissecting the Enthalpies of Vaporization. *ChemPhysChem* **2008**, *9*, 549–555. [[CrossRef](#)]
44. Chaban, V.; Voroshylova, I.V. Systematic Refinement of Canongia Lopes-Pádua Force Field for Pyrrolidinium-Based Ionic Liquids. *J. Phys. Chem. B* **2015**, *119*, 6242–6249. [[CrossRef](#)]
45. Barbosa, G.D.; Liu, X.; O'Hara, K.E.; Bara, J.E.; Turner, C.H. Charge scaling parameter evaluation for multivalent ionic liquids with fixed point charge force fields. *J. Ion. Liq.* **2022**, *2*, 100020. [[CrossRef](#)]
46. van der Spoel, D.; Lindahl, E.; Hess, B.; Groenhof, G.; Mark, A.E.; Berendsen, H.J.C. GROMACS: Fast, Flexible and Free. *J. Comp. Chem.* **2005**, *26*, 1701–1719. [[CrossRef](#)] [[PubMed](#)]
47. Lindahl, E.; Abraham, M.J.; Hess, B.; van der Spoel, D. Gromacs 2020-3 Version. Available online: <https://zenodo.org/record/3923644#.ZD9WLFzByUI> (accessed on 26 February 2023).
48. Chen, J.; Mia, J.G.; Chan, K.Y. Comparison of different mixing rules for prediction of density and residual internal energy of binary and ternary Lennard-Jones mixtures. *Fluid Phase Equilibria* **2001**, *178*, 87–95. [[CrossRef](#)]
49. Essman, U.; Perera, L.; Berkowitz, M.L.; Darden, T.; Lee, H.; Pedersen, L.G. A smooth particle mesh Ewald method. *J. Chem. Phys.* **1995**, *103*, 8577–8592. [[CrossRef](#)]
50. Hess, B.; Bekker, H.; Berendsen, H.J.C.; Fraaije, J.G.E.M. LINCS: A Linear Constraint Solver for molecular simulations. *J. Comp. Chem.* **1997**, *18*, 1463–1472. [[CrossRef](#)]
51. *Avogadro: An Open-Source Molecular Builder and Visualization Tool*; Version 1.2.0. Available online: <http://avogadro.cc/> (accessed on 26 February 2023).
52. Hanwell, M.D.; Curtis, D.E.; Lonie, D.C.; Vandermeersch, T.; Zurek, E.; Hutchison, G.R. Avogadro: An advanced semantic chemical editor, visualization, and analysis platform. *J. Cheminform.* **2012**, *4*, 1–17. [[CrossRef](#)]
53. Neese, F. The ORCA program system. *Wiley Interdiscip. Rev. Comput. Mol. Sci.* **2003**, *2*, 73–78. [[CrossRef](#)]
54. Johnson, E.R.; Becke, A.D. A post-Hartree-Fock model of intermolecular interactions. *J. Chem. Phys.* **2005**, *123*, 024101. [[CrossRef](#)] [[PubMed](#)]
55. Hehre, W.J.; Ditchfield, R.; Pople, J.A. Self-consistent molecular orbital methods. XII. Further extensions of Gaussian-type basis sets for use in molecular orbital studies of organic molecules. *J. Chem. Phys.* **1972**, *56*, 2257–2261. [[CrossRef](#)]

56. Breneman, C.M.; Wilberg, K.B. Determining Atom-Centered Monopoles from Molecular Electrostatic Potentials. The Need for High Sampling Density in Formamide Conformational Analysis. *J. Comput. Chem.* **1990**, *11*, 361–373. [[CrossRef](#)]
57. Bussi, G.; Donadio, D.; Parrinello, M. Canonical sampling through velocity rescaling. *J. Chem. Phys.* **2007**, *126*, 014101. [[CrossRef](#)]
58. Berendsen, H.J.C.; Postma, J.P.M.; DiNola, A.; Haak, J.R. Molecular dynamics with coupling to an external bath. *J. Chem. Phys.* **1984**, *81*, 3684–3690. [[CrossRef](#)]
59. Parrinello, M.; Rahman, A. Polymorphic transitions in single crystals: A new molecular dynamics method. *J. Appl. Phys.* **1981**, *52*, 7182–7190. [[CrossRef](#)]
60. Golding, J.; Hamid, N.; MacFarlane, D.R.; Forsyth, M.; Forsyth, C.; Collings, C.; Huang, J. N-Methyl-N-alkylpyrrolidinium Hexafluorophosphate Salts: Novel Molten Salts and Plastic Crystal Phases. *Chem. Mater.* **2001**, *13*, 558–564. [[CrossRef](#)]
61. Forsyth, S.; Golding, J.; MacFarlane, D.R.; Forsyth, M. N-methyl-N-alkylpyrrolidinium tetrafluoroborate salts: Ionic solvents and solid electrolytes. *Electrochim. Acta* **2001**, *46*, 1753–1757. [[CrossRef](#)]
62. Li, S.; Bañuelos, J.L.; Guo, J.; Anovitz, L.; Rother, G.; Shaw, R.W.; Hillesheim, P.C.; Dai, S.; Baker, G.A.; Cummings, P.T. Alkyl Chain Length and Temperature Effects on Structural Properties of Pyrrolidinium-Based Ionic Liquids: A Combined Atomistic Simulation and Small-Angle X-ray Scattering Study. *J. Phys. Chem. Lett.* **2012**, *3*, 125–130. [[CrossRef](#)]
63. Nasrabadi, A.T.; Gelb, L.D. Structural and Transport Properties of Tertiary Ammonium Triflate Ionic Liquids: A Molecular Dynamics Study. *J. Phys. Chem. B* **2017**, *121*, 1908–1921. [[CrossRef](#)]
64. Lourenço, T.C.; Zhang, Y.; Costa, L.T.; Maginn, E.J. A molecular dynamics study of lithium-containing aprotic heterocyclic ionic liquid electrolytes. *J. Chem. Phys.* **2018**, *148*, 193834. [[CrossRef](#)]
65. Tong, J.; Xiao, X.; Liang, X.; von Solms, N.; Huo, F.; He, H.; Zhang, S. Insights into the solvation and dynamic behaviors of a lithium salt in organic and ionic liquid-based electrolytes. *Phys. Chem. Chem. Phys.* **2019**, *21*, 19216–19225. [[CrossRef](#)]
66. Yamaguchi, S.; Yamada, H.; Takeoka, Y.; Rikukawa, M.; Yoshizawa-Fugita, M. Synthesis of pyrrolidinium-based plastic crystals exhibiting high ionic conductivity at ambient temperature. *New J. Chem.* **2019**, *43*, 4008–4012. [[CrossRef](#)]
67. Tong, J.; Wu, S.; von Solms, N.; Liang, X.; Huo, F.; Zhou, H.; Zhang, S. The Effect of Concentration of Lithium Salt on the Structural and Transport Properties of Ionic Liquid-Based Electrolytes. *Front. Chem.* **2020**, *7*, 945. [[CrossRef](#)]
68. Kashyap, H.K.; Santos, C.S.; Murthy, N.S.; Hettige, J.J.; Kerr, K.; Ramati, S.; Gwon, J.; Gohdo, M.; Lall-Ramnarine, I.; Wishart, J.F.; et al. Structure of 1-Alkyl-1-methylpyrrolidinium Bis(trifluoromethylsulfonyl)amide Ionic Liquids with Linear, Branched, and Cyclic Alkyl Groups. *J. Phys. Chem. B* **2013**, *117*, 15328–15337. [[CrossRef](#)]
69. Saitoh, K.; Takai, Y.; Sato, T.; Takuma, M.; Takahashi, Y. Optimization of LIB Electrolyte and Exploration of Novel Compounds via the Molecular Dynamics Method. *Batteries* **2022**, *8*, 27. [[CrossRef](#)]

Disclaimer/Publisher's Note: The statements, opinions and data contained in all publications are solely those of the individual author(s) and contributor(s) and not of MDPI and/or the editor(s). MDPI and/or the editor(s) disclaim responsibility for any injury to people or property resulting from any ideas, methods, instructions or products referred to in the content.